Crystal structure of gepirone, $C_{19}H_{29}N_5O_2$

James A. Kaduk [1,2,a], Anja Dosen [3] and Thomas N. Blanton [3]
[1]*Illinois Institute of Technology, 3101 S. Dearborn St., Chicago, IL 60616, USA*
[2]*North Central College, 131 S. Loomis St., Naperville, IL 60540, USA*
[3]*ICDD, 12 Campus Blvd., Newtown Square, PA 19073-3273, USA*

(Received 20 June 2024; accepted 10 September 2024)

The crystal structure of gepirone has been solved and refined using synchrotron X-ray powder diffraction data and optimized using density functional theory techniques. Gepirone crystallizes in space group $P2_1/a$ (#14) with $a = 16.81794(14)$, $b = 11.71959(5)$, $c = 10.10195(4)$ Å, $\beta = 95.7012(5)°$, $V = 1981.239(14)$ Å^3, and $Z = 4$ at 298 K. The crystal structure consists of discrete gepirone molecules. There are no classical hydrogen bonds in the crystal structure, but several intra- and intermolecular C–H···N and C–H···O hydrogen bonds contribute to the lattice energy. The powder pattern has been submitted to ICDD® for inclusion in the Powder Diffraction File™ (PDF®).

[doi:10.1017/S0885715624000514]

Key words: gepirone, Exxua, crystal structure, Rietveld refinement, density functional theory

I. INTRODUCTION

Gepirone (marketed under the trade name Exxua) is used for the treatment of adults with major depressive disorder and is being investigated for use in the treatment of general anxiety disorder. The systematic name (CAS Registry Number 83928-76-1) is 4,4-Dimethyl-1-(4-(4-(pyrimidin-2-yl)piperazin-1-yl)butyl)piperidine-2,6-dione. A two-dimensional molecular diagram of gepirone is shown in Figure 1.

Two polymorphs of gepirone hydrochloride had been known previously, and a third form was discovered by differential scanning calorimetry and thermal microscopy (Behme et al., 1985; Bristol-Myers). Single-crystal structures of Forms I and II of gepirone hydrochloride, as well as of gepirone-free base, were determined by Barbero (2019), but no atom coordinates were published.

This work was carried out as part of a project (Kaduk et al., 2014) to determine the crystal structures of large-volume commercial pharmaceuticals and include high-quality powder diffraction data for them in the Powder Diffraction File (Kabekkodu et al., 2024).

II. EXPERIMENTAL

Gepirone was a commercial reagent, purchased from TargetMol (Batch 156703), and was used as-received. The white powder was packed into a 0.5 mm diameter Kapton capillary and rotated during the measurement at ~2 Hz. The powder pattern was measured at 298(1) K at the BXDS-WLE Wiggler Low Energy Beamline (Leontowich et al., 2021) of the Brockhouse X-ray Diffraction and Scattering Sector of the Canadian Light Source using a wavelength of 0.819563(2) Å (15.1 keV) from 1.6 to 75.0° 2θ with a step size of 0.0025° and a collection time of 3 min. The high-resolution powder diffraction data were collected using eight Dectris Mythen2 X series 1 K linear strip detectors. NIST SRM 660b LaB_6 was used to calibrate the instrument and refine the monochromatic wavelength used in the experiment.

The pattern was indexed with DICVOL06 (Louër and Boultif, 2007) as incorporated into EXPO2014 (Altomare et al., 2013) on a primitive monoclinic unit cell with $a = 16.81970$, $b = 11.72400$, $c = 10.10370$ Å, $\beta = 95.702°$, $V = 1982.5$ Å^3, and $Z = 4$. The suggested space group was $P2_1/a$, which was confirmed by the successful solution and refinement of the structure. A reduced cell search of the Cambridge Structural Database (Groom et al., 2016) yielded 20 hits but no gepirone derivatives.

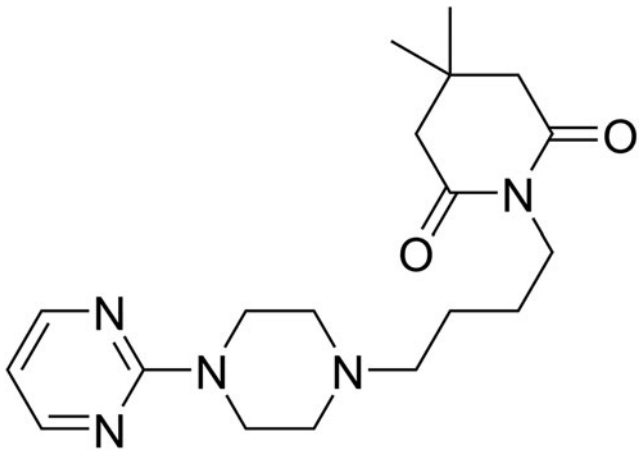

Figure 1. The two-dimensional structure of gepirone.

[a]Author to whom correspondence should be addressed. Electronic mail: kaduk@polycrystallography.com

The structure was solved by direct methods as implemented in EXPO2014 (Altomare et al., 2013) using the COVMAP option. A few atom types had to be reassigned manually. The initial hydrogen atom positions were calculated using Mercury (Macrae et al., 2020).

Rietveld refinement was carried out with GSAS-II (Toby and Von Dreele, 2013). Only the 3.5–50° portion of the pattern was included in the refinements ($d_{min} = 0.969$ Å). All non-H bond distances and angles were subjected to restraints based on a Mercury/Mogul Geometry Check (Bruno et al., 2004; Sykes et al., 2011). The Mogul average and standard deviation for each quantity were used as the restraint parameters. The pyrimidine ring was restrained to be planar. The restraints contributed 4.2% to the overall χ^2. The hydrogen atoms were included in calculated positions, which were recalculated during the refinement using the AddH item in Materials Studio (Dassault Systèmes, 2023); these H positions are calculated using a force field, so the X–H distances are longer than the usual crystallographic ones. The U_{iso} of the heavy atoms were grouped by chemical similarity. The U_{iso} for the H atoms were fixed at 1.3× the U_{iso} of the heavy atoms to which they are attached. The peak profiles were described using the generalized microstrain model (Stephens, 1999). The background was modeled using a 3-term shifted Chebyshev polynomial, with peaks at 10.38 and 41.94° to model the scattering from the Kapton capillary and an amorphous component.

The final refinement of 103 variables using 18,601 observations and 68 restraints yielded the residual $R_{wp} = 0.0445$. The largest peak (2.33 Å from C22) and hole (1.92 Å from O2) in the difference Fourier map were 0.32(9) and −0.34(9) eÅ^{-3}, respectively. The final Rietveld plot is shown in Figure 2. The largest features in the normalized error plot are in the shapes of some of the low-angle peaks and a few trace impurity peaks.

The crystal structure of gepirone was optimized (fixed experimental unit cell) with density functional theory techniques using VASP (Kresse and Furthmüller, 1996) through the MedeA graphical interface (Materials Design, 2024). The calculation was carried out on 32 cores of a 144-core (768 Gb memory) HPE Superdome Flex 280 Linux server at North Central College. The calculation used the GGA-PBE functional, a plane wave cutoff energy of 400.0 eV, and a k-point spacing of 0.5 Å^{-1} leading to a 2 × 2 × 2 mesh, and took ~15.5 h. Single-point density functional theory calculations (fixed experimental cell) and population analysis were carried out using CRYSTAL23 (Erba et al., 2023). The basis sets for the H, C, N, and O atoms in the calculation were those of Gatti et al. (1994). The calculations were run on a 3.5 GHz PC using 8 k-points and the B3LYP functional and took ~4.5 h.

III. RESULTS AND DISCUSSION

The powder pattern of this study is similar enough to that reported by Barbero (2019) to conclude that they represent the same material (Figure 3). Further confirmation is provided by the similarities of the lattice parameters (Table I). The small differences presumably reflect the differences in the temperatures of data collection (298 in this study and 293 K for Barbero). The root-mean-square Cartesian displacement of the non-H atoms in the Rietveld-refined and VASP-optimized molecules is 0.055 Å (Figure 4). The agreement is within the normal range for correct structures (van de Streek and Neumann, 2014). The asymmetric unit is illustrated in Figure 5. The remaining discussion will emphasize the VASP-optimized structure.

All bond distances, bond angles, and torsion angles fall within the normal ranges indicated by a Mercury Mogul Geometry check (Macrae et al., 2020). Quantum chemical geometry optimization of the isolated molecule (DFT/B3LYP/6-31G*/water) using Spartan '24 (Wavefunction, 2023) indicated that the gepirone molecule is essentially in a

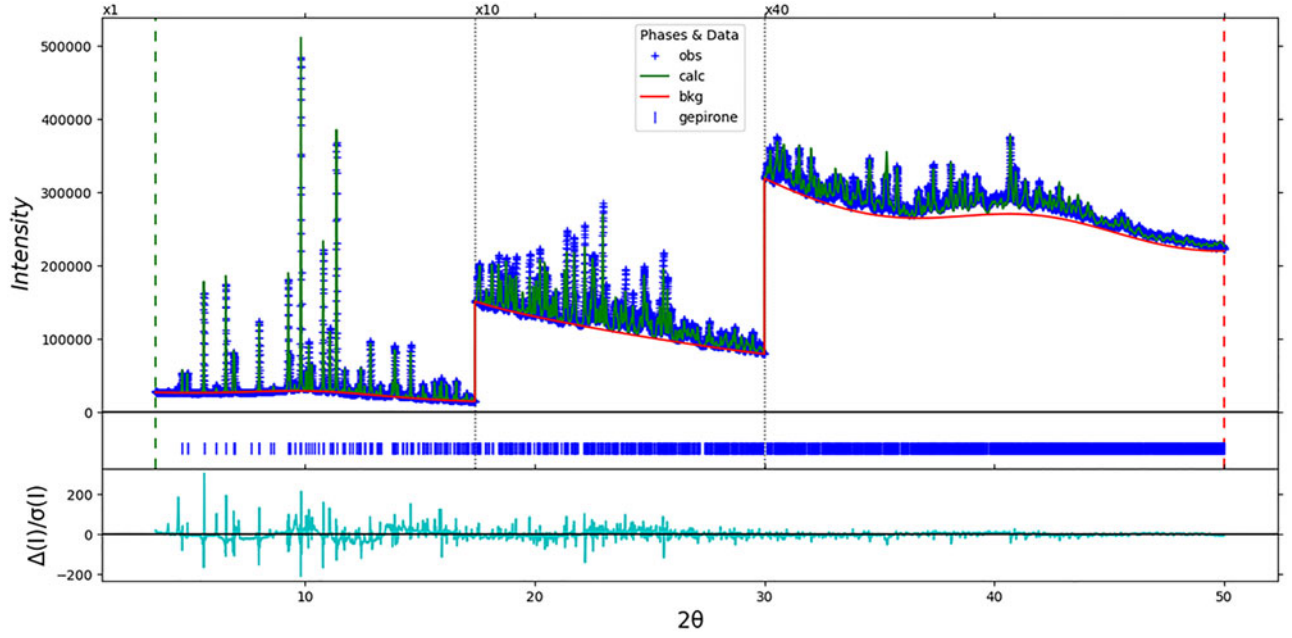

Figure 2. The Rietveld plot for the refinement of gepirone. The blue crosses represent the observed data points, and the green line is the calculated pattern. The cyan curve is the normalized error plot, and the red line is the background curve. The vertical scale has been multiplied by a factor of 10× for $2\theta > 17.4°$ and by a factor of 40× for $2\theta > 30.0°$.

https://doi.org/10.1017/S0885715624000514 Published online by Cambridge University Press

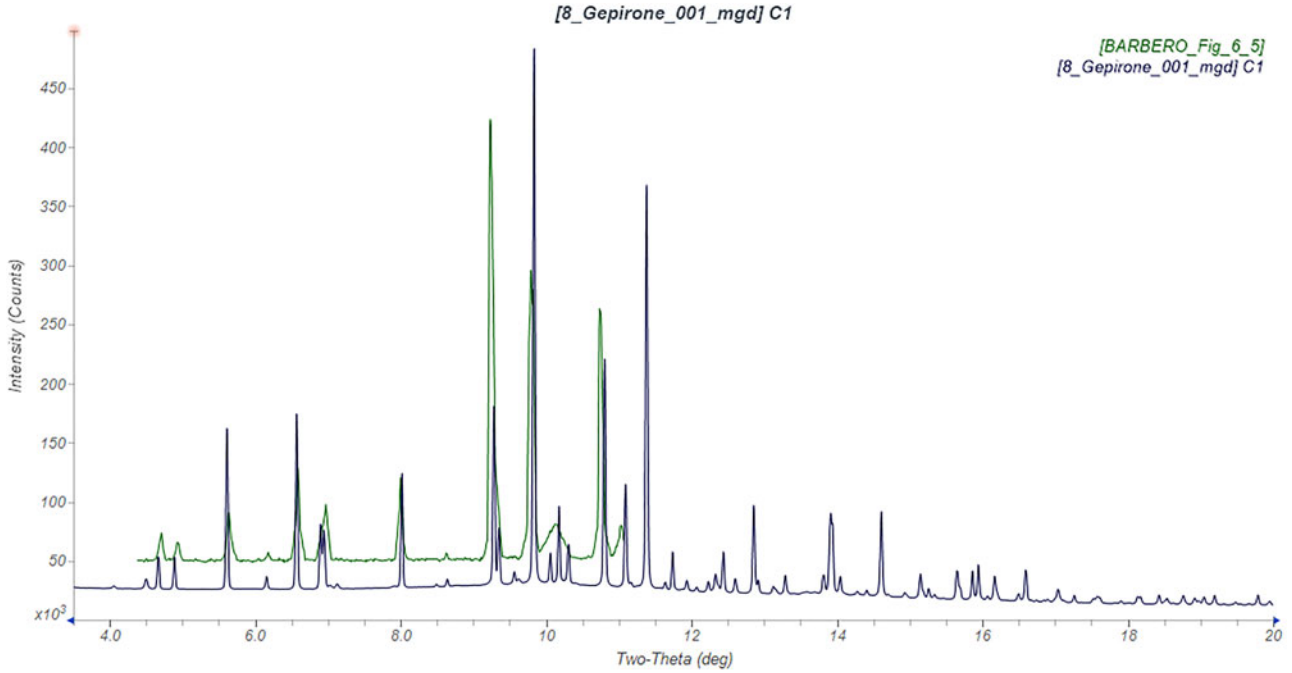

Figure 3. Comparison of the synchrotron pattern of gepirone (black) to that reported by Barbero (2019; green). The literature pattern (measured using Cu K_α radiation) was digitized using UN-SCAN-IT (Silk Scientific, 2013) and converted to the synchrotron wavelength of 0.819563(2) Å using JADE Pro (MDI, 2024). Image generated using JADE Pro (MDI, 2024).

TABLE I. Lattice parameters ($P2_1/a$) of gepirone.

Source	a (Å)	b (Å)	c (Å)	β (°)	V (Å^3)
This work	16.81793(14)	11.71959(5)	10.10195(4)	95.7012(5)	1981.238(14)
Barbero	16.800(3)	11.7068(19)	10.1000(16)	95.718(3)	1976.5(5)

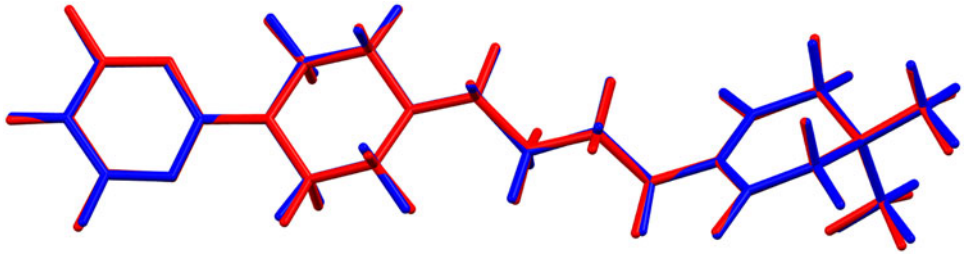

Figure 4. Comparison of the Rietveld-refined (red) and VASP-optimized (blue) structures of gepirone. The root-mean-square Cartesian displacement is 0.055 Å. Image generated using Mercury (Macrae et al., 2020).

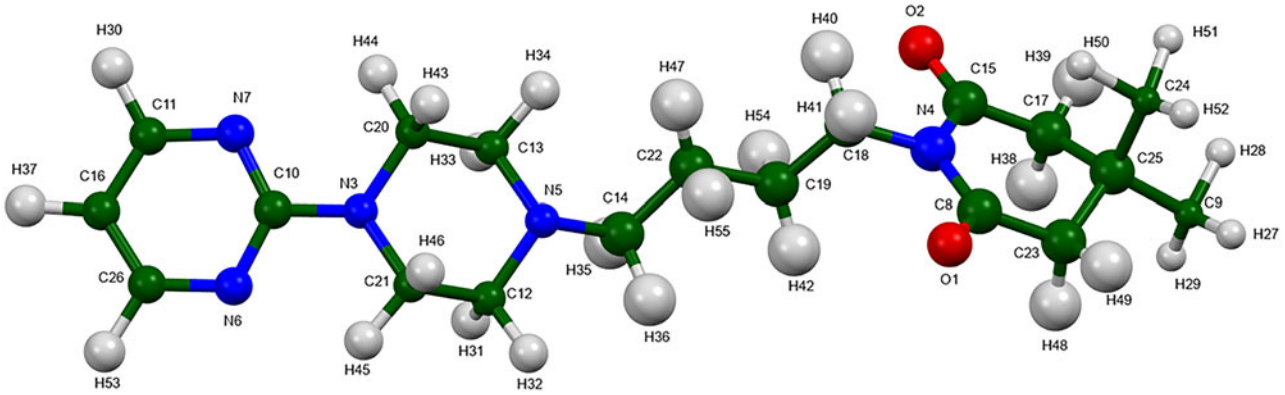

Figure 5. The asymmetric unit of gepirone, with the atom numbering. The atoms are represented by 50% probability spheroids. Image generated using Mercury (Macrae et al., 2020).

https://doi.org/10.1017/S0885715624000514 Published online by Cambridge University Press

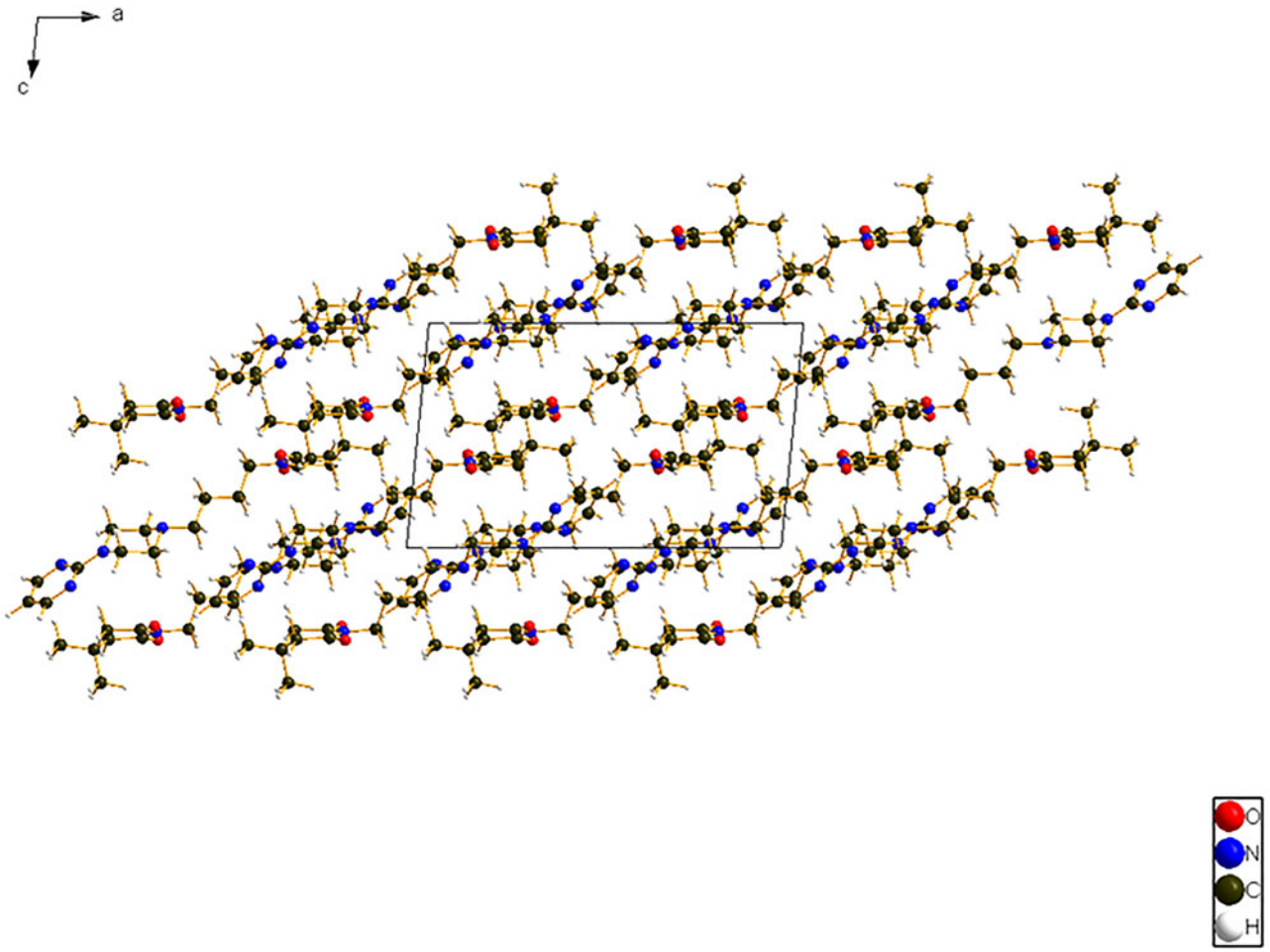

Figure 6. The crystal structure of gepirone, viewed down the *b*-axis. Image generated using Diamond (Crystal Impact, 2023).

local minimum-energy conformation; the rms Cartesian displacement is 0.298 Å. The global minimum-energy conformation is much more compact (folded on itself), indicating that intermolecular interactions are important to determining the solid-state conformation.

The crystal structure (Figure 6) consists of discrete gepirone molecules. The mean planes of the pyrimidine, piperazine, and piperidone dione rings are approximately −11,−6,−4; −4,−7,−12; and −3,2,−11, respectively. The mean plane of the entire molecule is approximately −4,−1,−5. There are no particularly strong aromatic–aromatic interactions; the shortest distance between the centroids of pyrimidine rings is 8.4 Å.

Analysis of the contributions to the total crystal energy of the structure using the Forcite module of Materials Studio (Dassault Systèmes, 2023) indicates that torsion, angle, and bond distortion terms are small and contribute about equally to the intramolecular energy (58.2 kcal/mol). The intermolecular energy is dominated by electrostatic attractions, which, in this force-field-based analysis, include hydrogen bonds. The hydrogen bonds are better discussed using the results of the density functional theory (DFT) calculation.

There are no classical hydrogen bonds in the crystal structure (Table II), but several intra- and intermolecular C–H···N and C–H–O hydrogen bonds contribute to the lattice energy.

The volume enclosed by the Hirshfeld surface of gepirone (Figure 7, Hirshfeld, 1977; Spackman et al., 2021) is 487.19 $Å^3$, which consitutes 98.36% of 1/4 of the unit cell volume. The packing density is thus fairly typical. The only significant close contacts (red in Figure 7) involve the hydrogen bonds. The volume/non-hydrogen atom is larger than normal, measuring 19.0 $Å^3$.

The Bravais–Friedel–Donnay–Harker (Bravais, 1866; Friedel, 1907; Donnay and Harker, 1937) morphology suggests that we might expect isotropic morphology for gepirone. A second-order spherical harmonic model was included in the refinement. The texture index was 1.005(0), indicating that the

TABLE II. Hydrogen bonds (CYSTAL23) in gepirone.

H-bond	D–H (Å)	H···A (Å)	D···A (Å)	D–H···A (°)	Overlap (*e*)
C23–H48···N5	1.112	2.480	3.578	169.2	0.036
C21–H45···N6	1.094	2.282[a]	2.768	104.6	0.015
C11–H30···N7	1.095	2.652	3.487	132.5	0.014
C18–H40···O2	1.096	2.269[a]	2.738	103.3	0.015
C23–H49···O2	1.100	2.622	3.683	161.8	0.014
C24–H51···O1	1.099	2.591	3.595	151.4	0.013
C2–H43···O1	1.106	2.552	3.657	178.1	0.012
C18–H41···O1	1.099	2.388[a]	2.700	94.1	0.010

[a]intramolecular

https://doi.org/10.1017/S0885715624000514 Published online by Cambridge University Press

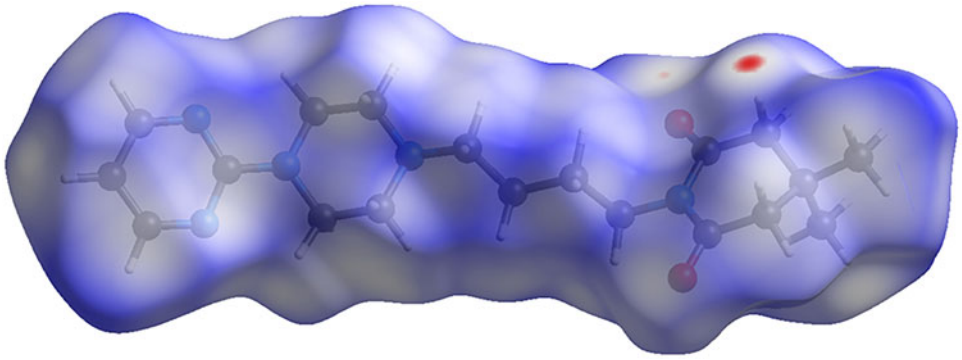

Figure 7. The Hirshfeld surface of gepirone. Intermolecular contacts longer than the sums of the van der Waals radii are colored blue, and contacts shorter than the sums of the radii are colored red. Contacts equal to the sums of radii are white. Image generated using CrystalExplorer (Spackman et al., 2021).

preferred orientation was insignificant in this rotated capillary specimen.

IV. DEPOSITED DATA

The powder pattern of gepirone from this synchrotron data set has been submitted to ICDD for inclusion in the Powder Diffraction File. The Crystallographic Information Framework (CIF) files containing the results of the Rietveld refinement (including the raw data) and the DFT geometry optimization were deposited with the ICDD. The data can be requested at pdj@icdd.com.

Acknowledgements

The synchrotron data collection described in this paper was performed at the Canadian Light Source (CLS), a national research facility of the University of Saskatchewan, which is supported by the Canada Foundation for Innovation (CFI), the Natural Sciences and Engineering Research Council (NSERC), the Canadian Institute of Health Research (CIHR), the Government of Saskatchewan, and the University of Saskatchewan. This work was partially supported by the International Centre for Diffraction Data. We thank Adam Leontowich (CLS) for his assistance in the synchrotron data collection and Megan Rost (ICDD) for laboratory data collection before the gepirone specimen was sent to CLS.

Conflicts of interest

The authors have no conflicts of interest to declare.

REFERENCES

Altomare, A., C. Cuocci, C. Giacovazzo, A. Moliterni, R. Rizzi, N. Corriero, and A. Falcicchio. 2013. "EXPO2013: A Kit of Tools for Phasing Crystal Structures from Powder Data." *Journal of Applied Crystallography* 46: 1231–5.

Barbero, M. 2019. "Chemistry of APIs: Synthesis and Solid-State Properties." Ph.D. Dissertation. Novara, Italy: Università del Piemonte Orientale "Amedeo Avogadro ".

Behme, R. J., D. Brooke, R. F. Farney, and T. T. Kensler. 1985. "Characterization of Polymorphism of Gepirone Hydrochloride." *Journal of Pharmaceutical Sciences* 74: 1041–46.

Bravais, A. 1866. *Etudes Cristallographiques*. Paris, Gauthier Villars.

Bruno, I. J., J. C. Cole, M. Kessler, J. Luo, W. D. S. Motherwell, L. H. Purkis, B. R. Smith, R. Taylor, R. I. Cooper, S. E. Harris, and A. G. Orpen. 2004. "Retrieval of Crystallographically-Derived Molecular Geometry Information." *Journal of Chemical Information and Computer Sciences* 44: 2133–44.

Crystal Impact. 2023. *Diamond V. 5.0.0*. Bonn, Germany, Crystal Impact - Dr. H. Putz & Dr. K. Brandenburg.

Dassault Systèmes. 2023. *BIOVIA Materials Studio 2024*. San Diego, CA, BIOVIA.

Donnay, J. D. H., and D. Harker. 1937. "A New Law of Crystal Morphology Extending the Law of Bravais." *American Mineralogist* 22: 446–67.

Erba, A., J. K. Desmarais, S. Casassa, B. Civalleri, L. Donà, I. J. Bush, B. Searle, L. Maschio, L.-E. Daga, A. Cossard, C. Ribaldone, E. Ascrizzi, N. L. Marana, J.-P. Flament, and B. Kirtman. 2023. "CRYSTAL23: A Program for Computational Solid State Physics and Chemistry." *Journal of Chemical Theory and Computation* 19: 6891–932. doi:10.1021/acs.jctc.2c00958.

Friedel, G. 1907. "Etudes sur la loi de Bravais." *Bulletin de la Société Française de Minéralogie* 30: 326–455.

Gatti, C., V. R. Saunders, and C. Roetti. 1994. "Crystal-Field Effects on the Topological Properties of the Electron-Density in Molecular Crystals - the Case of Urea." *Journal of Chemical Physics* 101: 10686–96.

Groom, C. R., I. J. Bruno, M. P. Lightfoot, and S. C. Ward. 2016. "The Cambridge Structural Database." *Acta Crystallographica Section B: Structural Science, Crystal Engineering and Materials* 72: 171–9.

Hirshfeld, F. L. 1977. "Bonded-Atom Fragments for Describing Molecular Charge Densities." *Theoretica Chemica Acta* 44: 129–38.

Kabekkodu, S., A. Dosen, and T. N. Blanton. 2024. "PDF-5+: A Comprehensive Powder Diffraction File™ for Materials Characterization." *Powder Diffraction* 39: 47–59.

Kaduk, J. A., C. E. Crowder, K. Zhong, T. G. Fawcett, and M. R. Suchomel. 2014. "Crystal Structure of Atomoxetine Hydrochloride (Strattera), $C_{17}H_{22}NOCl$." *Powder Diffraction* 29: 269–73.

Kresse, G., and J. Furthmüller. 1996. "Efficiency of Ab-Initio Total Energy Calculations for Metals and Semiconductors Using a Plane-Wave Basis Set." *Computational Materials Science* 6: 15–50.

Leontowich, A. F. G., A. Gomez, B. Diaz Moreno, D. Muir, D. Spasyuk, G. King, J. W. Reid, C.-Y. Kim, and S. Kycia. 2021. "The Lower Energy Diffraction and Scattering Side-Bounce Beamline for Materials Science at the Canadian Light Source." *Journal of Synchrotron Radiation* 28: 961–9.

Louër, D., and A. Boultif. 2007. "Powder Pattern Indexing and the Dichotomy Algorithm." *Zeitschrift für Kristallographie Supplement* 26: 191–6.

Macrae, C. F., I. Sovago, S. J. Cottrell, P. T. A. Galek, P. McCabe, E. Pidcock, M. Platings, G. P. Shields, J. S. Stevens, M. Towler, and P. A. Wood. 2020. "Mercury 4.0: From Visualization to Design and Prediction." *Journal of Applied Crystallography* 53: 226–35.

Materials Design. 2024. *MedeA 3.7.2*. San Diego, CA, Materials Design Inc.

MDI. 2024. *JADE Pro Version 9.0*. Livermore, CA, Materials Data.

Silk Scientific. 2013. *UN-SCAN-IT 7.0*. Orem, UT, Silk Scientific Corporation.

https://doi.org/10.1017/S0885715624000514 Published online by Cambridge University Press

Spackman, P. R., M. J. Turner, J. J. McKinnon, S. K. Wolff, D. J. Grimwood, D. Jayatilaka, and M. A. Spackman. 2021. "Crystalexplorer: A Program for Hirshfeld Surface Analysis, Visualization and Quantitative Analysis of Molecular Crystals." *Journal of Applied Crystallography* 54: 1006–11. doi:10.1107/S1600576721002910.

Stephens, P. W. 1999. "Phenomenological Model of Anisotropic Peak Broadening in Powder Diffraction." *Journal of Applied Crystallography* 32: 281–9.

Sykes, R. A., P. McCabe, F. H. Allen, G. M. Battle, I. J. Bruno, and P. A. Wood. 2011. "New Software for Statistical Analysis of Cambridge Structural Database Data." *Journal of Applied Crystallography* 44: 882–6.

Toby, B. H., and R. B. Von Dreele. 2013. "GSAS II: The Genesis of a Modern Open Source All Purpose Crystallography Software Package." *Journal of Applied Crystallography* 46: 544–9.

van de Streek, J., and M. A. Neumann. 2014. "Validation of Molecular Crystal Structures from Powder Diffraction Data with Dispersion-Corrected Density Functional Theory (DFT-D)." *Acta Crystallographica Section B: Structural Science, Crystal Engineering and Materials* 70: 1020–32.

Wavefunction, Inc. 2023. *Spartan '24. V. 1.0.0*. Irvine, CA, Wavefunction Inc.

https://doi.org/10.1017/S0885715624000514 Published online by Cambridge University Press